2018 IEEE Intelligent Vehicles Symposium (IV)
Changshu, Suzhou, China, June 26-30, 2018

Naturalistic Lane Change Analysis for Human-Like Trajectory Generation

Donghao Xu, Zhezhang Ding, Huijing Zhao, Mathieu Moze, François Aioun, and Franck Guillemard

Abstract— **Human-like driving is of great significance for safety and comfort of autonomous vehicles, but existing trajectory planning methods for on-road vehicles rarely take the similarity with human behavior into consideration. From a representative trajectory-generation-based planning algorithm, this paper analyzes the systematic deviation of the generated trajectories from human trajectories, and proposes a new scheme of trajectory generation by compensating the deviation using a deviation profile learned from data. Experimental results show that the proposed trajectory generator is able to fit the human trajectories considerably better than the original one with only one additional degree of freedom. When used for online trajectory planning, with the same level of computational complexity, the proposed generator is able to generate trajectories that are more human-like than original generator does, which provides basis for autonomous vehicle to perform human-like trajectory planning.**

I. Introduction

Last decade has witnessed tremendous progress in the field of autonomous driving. Many prototyping vehicles have been demonstrated [1][2][3], Advanced Driving Assistant Systems (ADAS) are being evolved from information assistance to automated driving [4], and commercial cars with conditional autonomous functions have been produced.

Motion planning is a key component of these systems, which generates a kinematically and dynamically feasible trajectory by addressing both path and velocity for the vehicle to track on, and therefore greatly affect the performance of its intelligent behavior. Headway management and lane change are the major behaviors during highway driving. Headway management such as lane keeping [5], car following [6] and platooning [7][8] have been extensively studied, and the techniques are used in developing Adaptive Cruise Control (ACC) systems. Lane change involves both longitudinal and lateral controls, and more importantly, the decision making and maneuvers are highly correlated with road and other traffic participants nearby [9][10]. It is therefore considered that lane change is more challenging, and its operation requires higher level intelligence of an autonomous driving system, especially in real-world traffic.

Motion planning for a lane change behavior is usually conducted by first generating a set of candidate trajectories, then selecting an optimal one for execution according to an evaluation function. As the parameter space of candidate trajectories could be high-dimensional, in order to reduce search space due to limited computation resources and real-time operation needs, a finite set of trajectories is generated by assuming on parametric models and linking an initial state to a set of local goals. In [11][12], 20-50 trajectories are generated by varying the goal points with different offsets from the center of the road, and 10 to 30 meters away from the vehicle. The model-predictive trajectory generator [13] is used to produce each dynamically feasible trajectory with assumptions on time-based linear velocity profiles and arclength-based curvature spline with three independent knot points (i.e. four degrees of freedom). Based on the jerk-optimal theory in [14], [15][16] formulates each candidate trajectory as a pair of quintic polynomials representing the lateral and longitudinal movements respectively. Each quintic polynomial is a function of time (i.e. a one-dimensional problem), and the coefficients are estimated by bounding on two terminal states at the Frenet-Frame [17]. Spatiotemporal state lattices are used to represent the configuration space in motion planning [18], and quintic polynomial trajectories are generated to link pairs of lattice points, where valid edges are only build if bound conditions on velocity, acceleration and jerk are met. In [19] trajectory rule templates are prepared in an offline procedure, which are selected during online motion planning to provide a copy set of trajectory candidates of the particular behavior undergoing. Curvature spline [13] or Bezier Curve [20] are used to estimate trajectories of each rule template.

Whereas trajectory generation has technological feasibility for achieving vehicle autonomy, the behavior could be much different from one of a human driver. Although comfort, as jerk, has been incorporated in evaluation functions [12][15][21][22] to select optimal trajectories from the candidate sets, few studies have been conducted to address human driving pattern at trajectory generation level. [23] analyzed human driving data to fit speed and path model parameters for traffic-free planning. [24] modeled lane change in two segments, and divided the behaviors into active and passive styles by analyzing distance and velocity parameters of human driving data. [25] sampled end states by analyzing the most usual terminal locations of human lane change trajectories, while quintic polynomials are assumed to link an initial state to each sampled end points.

This research seeks to answer the questions: how well does parametric lane change trajectory fit on human driver data? How to generate trajectory candidates that has both efficiency for planning and fitness to human driving styles? A lane change trajectory dataset during naturalistic on-road

This work is partially supported by PSA's OpenLab program (Multimodal Perception and Reasoning for Intelligent Vehicles) and the NSFC Grants 61573027. D. Xu, Z. Ding and H. Zhao are with the Key Lab of Machine Perception (MOE), Peking University, Beijing, China; M. Moze, F. Aioun and F. Guillemard are with Groupe PSA, Velizy, France.
Contact: H. Zhao, zhaohj@cis.pku.edu.cn.

human driving has been developed in the authors' early work [26]. These human lane change trajectories are analyzed by evaluating the fitting errors of a traditional trajectory generator [27] based on quintic polynomial with given bounding conditions, and a new trajectory generator with better fitting ability is proposed, which can generate trajectory sets with limited number of candidates for planning efficiency and improved ability of approximating human trajectories.

This paper is structured as follows. Section II performs data analysis to present the problem that current trajectory generator faces, then a new scheme for trajectory generation is proposed in section III and experiments are conducted to demonstrate its effectiveness in section IV. Finally, a conclusion is drawn in section V.

II. Problem Statement

A. Trajectory Generation for Planning

There is a category of trajectory planning methods for on-road vehicles in which candidate trajectories are first generated, then the one with the minimum cost is selected. Here we briefly review the scheme of lane change trajectory generation of the planning method in [27]. In this method, lateral and longitudinal motions of lane change procedure are modeled respectively and quintic polynomials are adopted to represent the trajectory, i.e.,

$$\begin{aligned} x(t) &= b_0 + b_1 t + b_2 t^2 + b_3 t^3 + b_4 t^4 + b_5 t^5 \\ y(t) &= c_0 + c_1 t + c_2 t^2 + c_3 t^3 + c_4 t^4 + c_5 t^5 \end{aligned} \tag{1}$$

where x and y represent the lateral and longitudinal directions respectively. Based on this representation, by adding constraints on motion states of start point and end point of a lane change procedure, the coefficients of the polynomials will be determined so that a trajectory is generated. When applied to straight lanes, the constraints on lateral motion include:

$$\begin{aligned} x(0) = 0, x'(0) = 0, x''(0) = 0 \\ x(T) = d, x'(T) = 0, x''(T) = 0 \end{aligned} \tag{2}$$

and the constraints on longitudinal motion include:

$$\begin{aligned} y(0) = 0, y'(0) = v_0, y''(0) = a_0 \\ y'(T) = v_T, y''(T) = 0, y'(T + \Delta t) = v_T \end{aligned} \tag{3}$$

where the start and end time of lane change are 0 and T respectively, and the location of start point is $(0, 0)$, and Δt is a small positive value. With these constraints, coefficients of the trajectory polynomial can be worked out by solving the linear equations.

When used for online planning, the lateral displacement d can be set fixed according to the central line of the target lane, and the longitudinal velocity and acceleration at start point (v_0 and a_0) are also available. Thus, candidate trajectories can be generated by first enumerating T and v_T on discrete grids then solving equations to obtain corresponding trajectory coefficients. It is worth noting that there is no constraint on the longitudinal displacement at end point. This is because the longitudinal displacement vary in such a large range that it cannot be enumerated with limited computation resource.

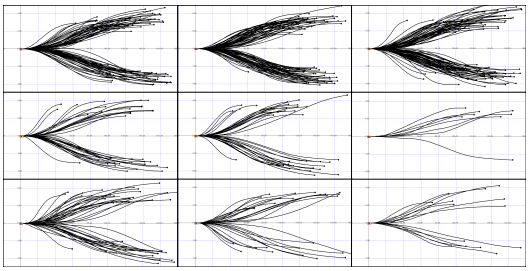

Fig. 1. Visualization of collected naturalistic lane change trajectories. All trajectories are divided into 9 subfigures according to their collection date.

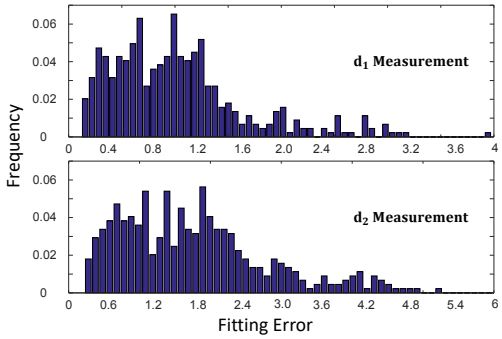

Fig. 2. Histogram of errors of fitting by the trajectory generator in II-A to human lane change trajectories. Top figure corresponds to error based on distance measurement d_1, and bottom figure corresponds to d_2 (refer to (4)).

B. Analysis of Deviation from Human Trajectories

In order to learn and perform a human-like planning based on the above framework, it needs to be ensured that in the generated candidate set, there is at least one trajectory close enough to the human driven trajectory. In our experiments, 444 lane change trajectories are used for analysis and they are collectively shown in Fig. 1. Below, we will examine if the existing trajectory generation method can meet the requirement.

1) Deviation statistics: The main procedure is as follows. First, generate an approximate trajectory for each human trajectory sample by assigning free parameters (v_T and T for the studied method) of the trajectory generator with corresponding values of the human trajectory. Then, for each trajectory sample, calculate the distance between the human trajectory and the approximate trajectory. The distance can be regarded as a fitting error. Finally, fitting errors of all samples are collected for statistical analysis. Note that the measurement of distance is not unique, so results based on two distance measurements will be presented and analyzed. The distance measurements adopted in our experiments are defined as follows:

$$\begin{aligned} d_1 &= \frac{1}{T}\int_0^T \left(\|v_1(t) - v_2(t)\| + \|p_1(t) - p_2(t)\|\right) dt \\ d_2 &= \max_{t\in[0,T]} \left(\|v_1(t) - v_2(t)\| + \|p_1(t) - p_2(t)\|\right) \end{aligned} \tag{4}$$

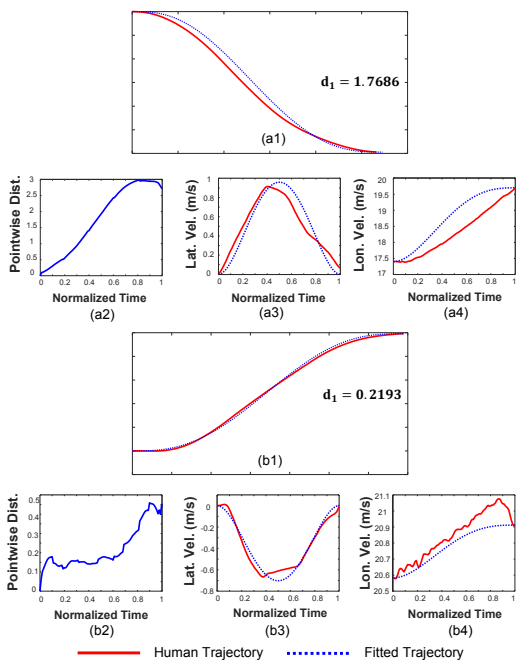

Fig. 3. Two cases of trajectory fitting errors. (·1) shows the shape of human trajectory and the generated trajectory. (·2) shows the pointwise distance over time. (·3) compares the lateral velocity of the two trajectories over time and (·4) does the same for longitudinal velocity.

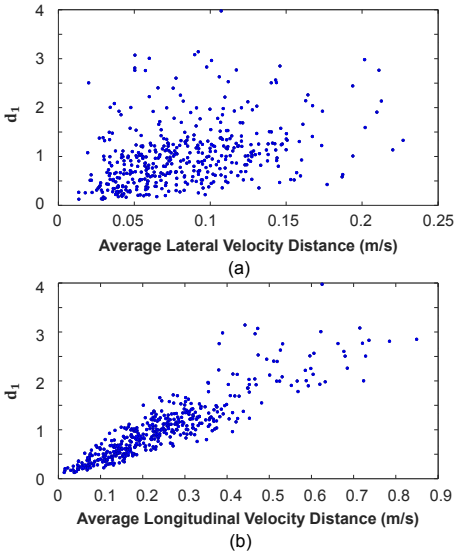

Fig. 4. Error samples for demonstrating correlation between the fitted error based on d_1 distance and the average velocity distance (top for lateral and bottom for longitudinal) between each human trajectory and the generated trajectory.

where $p_i(t)$ and $v_i(t)$ respectively represent the position and the velocity of trajectory i at time t. Besides, the formula $\|v_1(t) - v_2(t)\| + \|p_1(t) - p_2(t)\|$ is called as $pointwise\ distance$ at time t, which means d_1 represents mean of pointwise distance in $t \in [0, T]$, and d_2 shows the maximal value of pointwise distance in $t \in [0, T]$.

Statistical histograms of distance values (fitting errors) are presented in Fig. 2 to demonstrate the level of generated trajectories' deviation from human trajectories. From the figure, it can be deduced that the fitting error distributes in a quite wide range, and there are extreme cases with fitting errors 20 times higher than those well fitted (e.g., 4 vs 0.2 in Fig. 2 for d_1 measurement). In these cases, human trajectories cannot be well approximated by the generated ones, which makes it impossible to perform accurate human-like planning.

2) Deviation analysis by cases: To understand what leads to the deviation, two cases are presented for a detailed observation of trajectories with different levels of deviation. The first trajectory is shown in Fig. 3(a1), along with the generated trajectory, where it can be seen that there is not much difference between the shape of these two trajectories. However, if we examine the pointwise distance between them over time as shown in Fig. 3(a2), it will be found that the distance is increasing as time evolves, and the fitting error (d_1 distance between the human trajectory and the generated trajectory) is 1.7686, which indicates a relatively high level of deviation among all trajectory samples (refer to the histogram in Fig. 2). Fig. 3(a3) shows how lateral velocity develops over time of both human trajectory and the fitted trajectory, and (a4) shows that of longitudinal velocity. We see from (a3) that the overall trend of lateral velocity of the fitted trajectory does not deviate much from that of the human one. This is probably because when generating the lateral motion of a trajectory, the lateral displacement of the end point is taken as a constraint so that the accumulated error of lateral speed from the start point to the end point must be 0. However, as for longitudinal velocity shown in (a4), the human trajectory and the fitted generated trajectory go through quite different route: the instantaneous differences between their longitudinal velocities go over $0.7m/s$ at some moments.

As a comparison, the information of case 2 is plotted in the same way in Fig. 3(b1)-(b4). The d_1 distance between the human trajectory and the generated trajectory is 0.2193, which is much smaller values compared with that of case 1. From (b3), we see that the two lateral velocity curves also don't deviate much from each other, but in (b4), longitudinal velocity curve of the generated trajectory fits much better to that of the human trajectory: the instantaneous differences between their longitudinal velocities are no more than $0.2m/s$ at all moments.

These two cases imply that the fitting error may be dominated by the error of longitudinal velocity. To verify the assumption, we calculate fitting errors (d_1 distance from the generated trajectory to human trajectory) and average longitudinal velocity errors ($\frac{1}{T}\int_0^T \|v_1(t) - v_2(t)\|dt$) of all trajectory samples, and then plot all pairs of them in the 2-d plane as shown in Fig. 4(b), where we can see that samples of the two errors almost lie on a straight line, indicating strong linear correlation between them. The samples of fitting errors and lateral velocity errors are plotted in Fig. 4(a), where we can see that there is no clear correlation between these two

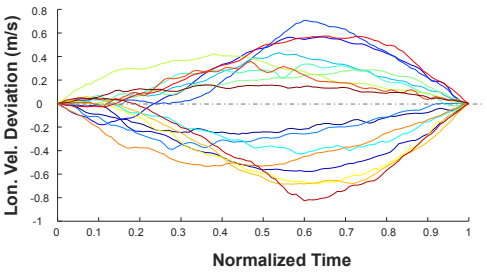

Fig. 5. Samples of the longitudinal velocity difference between human trajectories and generated trajectories. Notice the up-down and down-up pattern of the deviation curve.

errors. The phenomenon inspires us to introduce additional degrees of freedom to the original trajectory generator to compensate the longitudinal velocity error, so that the new trajectory generator is able to generate more human-like trajectories.

III. Human-Like Trajectory Generation

In order to approximate the human driving trajectories by generated ones, a new degree of freedom should be added to the original trajectory generator. We propose a scheme based on the trajectory generator in II-A. First, the deviation of longitudinal velocity between human driving trajectories and generated trajectories is modeled. Then, for online trajectory generation, trajectories with error compensation can be generated by eliminating the modeled deviation from trajectories produced by original generator with a proper scale parameter controlling the level of deviation.

Fig. 5 shows how the longitudinal velocity difference between generated trajectories and human driving trajectories develop over time (the time is normalized to the range [0,1] to align trajectories of various durations). In the figure, each curve corresponds to a trajectory sample, and the generated trajectory for comparison is generated as in II-A according to the state of start and end points of the human driving one. From the figure, we can see that the deviation curves of longitudinal velocity of different samples are similar in the way that they all follow the up-and-down or down-and-up pattern but with different scales. Thus, it's possible to model the deviation by formulating its profile and using a scale parameter to represent its level.

A. Deviation Modeling

In this part, the profile of deviation will first be mined out using principal component analysis and represented by sequential values on discrete time grids. Then, a polynomial will be fitted to the deviation sequence so that a smooth trajectory can be obtained.

1) PCA for longitudinal velocity deviation: For each lane change trajectory sample, a generated trajectory is first obtained as in II-A according to the start and end states of the human driving trajectory. Then, sequences of longitudinal velocity of the two trajectories are resampled uniformly as m points. Note that the resampled timestamps probably don't coincide with the original sampling points, so the resampling process needs interpolation of data. Then, the difference between the longitudinal velocity of human driving trajectory and the generated trajectory on the sampled m points are calculated and the obtained difference sequence can be regarded as a m-dimensional vector, which is called the deviation vector. Denoting the ith trajectory sample's deviation vector as x_i (column vector) and let $X = [x_1, \dots, x_N]$. Since the deviation goes over 0 or down below 0 almost symmetrically as shown in Fig. 5, we may as well let the mean of deviation vector be zero so that the modeling of deviation can be simplified. Under this assumption, the covariance matrix of deviation vectors can be computed as $C = XX^T$. Then, the eigenvector of C with the largest eigenvalue is the principal component the velocity deviation, i.e., the deviation profile.

2) Polynomial fitting of the deviation profile: Assume the time of all trajectories are normalized into $[0, 1]$. Then, the normalized timestamps of the deviation profile will be $t_k = k/(m-1), k = 0, \dots, m-1$. Denoting the value of kth dimension of deviation profile as e_k and the polynomial with coefficients w as $f(\cdot|w)$, then fitting the polynomial to the deviation profile is to solve the following optimization problem:

$$\begin{aligned} \min_{w} \quad & \sum_{k=1}^{m-2} \left(f(t_k|w) - e_k\right)^2 \\ \text{subject to} \quad & f(0|w) = 0, \\ & f(1|w) = 0 \end{aligned} \tag{5}$$

This is a quadratic optimization problem with linear equality constraints, which has a unique solution than can be represented analytically.

Denoting the obtained best value of w as w^*, then the polynomial representation of deviation profile is $f(t|w^*), t \in [0, 1]$. Note that when this deviation function is used for trajectory with end point at time T, it should correspondingly transformed into the interval $[0, T]$, i.e., $f(t/T|w^*), t \in [0, T]$.

B. Trajectory Generation with Error Compensation

To use the learned deviation profile for online lane change trajectory generation, additional to v_T and T (refer to II-A), a deviation scale α should also be enumerated. Concretely, for each generated trajectory by methods in II-A, we first calculate the deviation of displacement (denoted as $\Delta y(t)$) by integrating $f(t/T|w^*)$ with respect to t on $[0, T]$, then enumerate an α on predefined grids, and finally add the scaled displacement deviation to the original longitudinal motion equation $y_o(t)$ to get the motion equation with error compensation:

$$y(t) = y_o(t) + \alpha \cdot \Delta y(t) \tag{6}$$

IV. Experimental Results

A. Deviation Modeling

In our experiments, the number of resampled timestamps for deviation modeling is $m = 101$. Scatter plots in Fig. 6

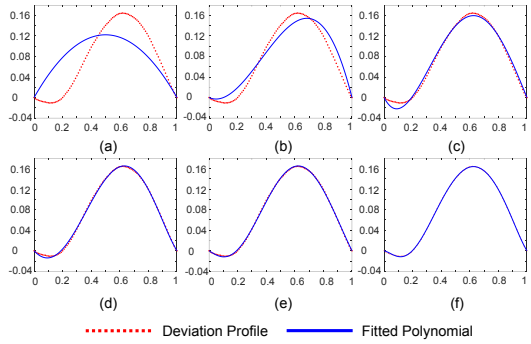

Fig. 6. Polynomial fitting results to the deviation profile. Results from 2nd-order to 7th-order fitting are presented in (a)-(f) respectively.

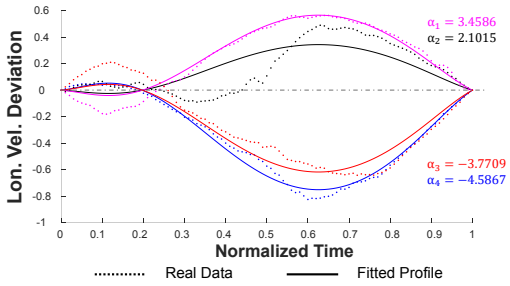

Fig. 7. Cases of longitudinal velocity deviation samples (dotted lines) fitted by the learned polynomial deviation profile (solid lines) with respective scale parameters.

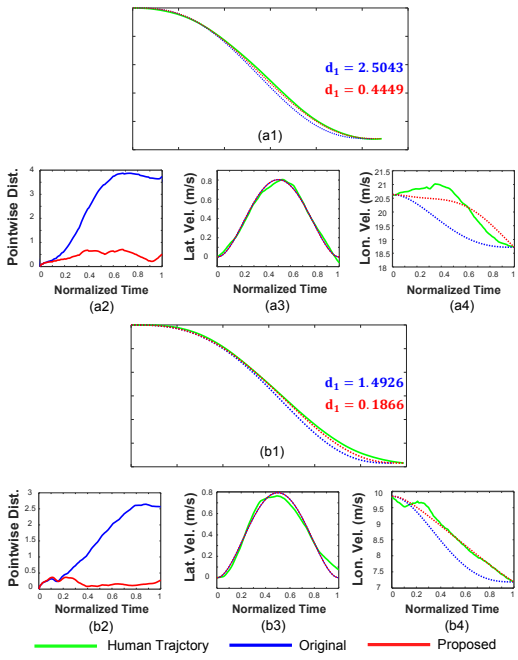

Fig. 9. Two cases of trajectory fitting errors of the original and proposed trajectory generator. (·1) shows the shape of human trajectory and generated trajectories. (·2) shows the pointwise distance over time. (·3) compares the lateral velocity of human and generated trajectories over time and (·4) does the same for longitudinal velocity. Note that in the lateral direction we keep the original method, and the distance of lateral velocity is quite small compared to the longitudinal one.

show the principal component of deviation, and continuous curves results of fitted deviation profiles by polynomials of various orders from 2 to 7. From the figure, we can see that the principal component of deviation can be fitted well with a 6th-order polynomial, which will be adopted in the following experiments.

Fig. 7 shows cases of deviations of trajectory samples (a subset of samples in Fig. 5) compared with deviations represented in best fitted polynomial with respective scales which are determined by calculating projected lengths of the deviation vectors on the deviation profile. From the figure, we can see that with a proper scale, the deviation can be fairly

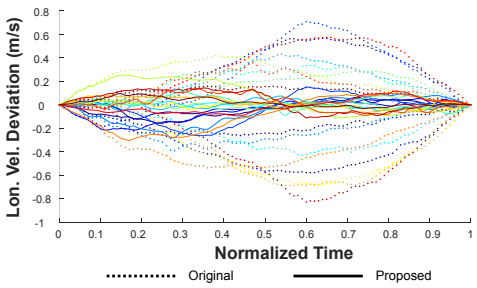

Fig. 8. Samples of longitudinal velocity deviation between human trajectory and generated trajectories from the original and proposed trajectory generator.

approximated, but some residual deviation of minor level still remains. The deviation curves of trajectories produced by the new generator are shown in Fig. 8, where dotted lines are copied from Fig. 5 for a clear comparison. Compared with Fig. 5, the range of deviation curves becomes much closer to 0.

In Fig. 9, two cases are shown with the same layout as in Fig. 3. In addition to the information of the human trajectory and the generated trajectory by the original generator, information of the generated trajectories by the proposed generator is also displayed. In each case, we see that the shape and longitudinal velocity of the generated trajectory from the proposed generator fit to those of the human trajectory much better than the original generator does, and the pointwise distance (error) to the human trajectory also implies considerable improvement of the proposed generator over the original one. Note that generation of approximate trajectories using the proposed generator also follows the principle in II-B(1), i.e., assigning free parameters of the generator with corresponding values of the human trajectory. Concretely speaking, for the proposed generator, v_T and T of the human trajectory are first used to generate a trajectory by the original generator, and then, a vector of longitudinal velocity deviation from the human trajectory is calculated and α is the projected length of the deviation vector on the deviation profile, and the final generated trajectory from the proposed generator can be obtained as introduced in III-B.

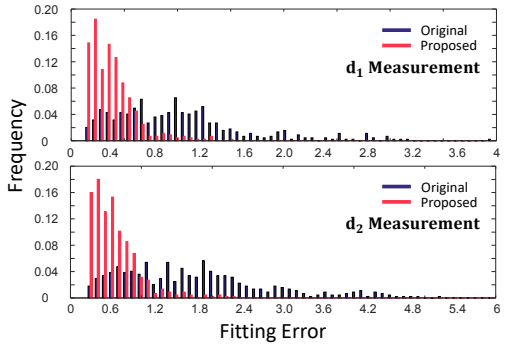

Fig. 10. Histogram of errors of fitting by original trajectory generator and proposed trajectory generator to human lane change trajectories.

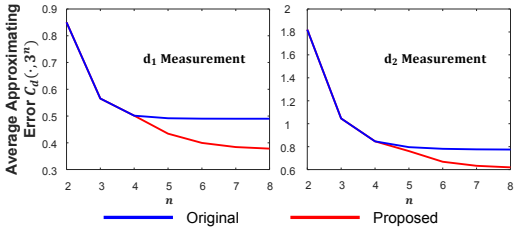

Fig. 11. Average approximating error of the original trajectory generator and the proposed trajectory generator under two distance measures (refer to (4)): (a) d_1 measurement and (b) d_2 measurement.

In conclusion, the deviation of original trajectory generator can be compensated with the learned deviation model with a proper scale parameter, so that the proposed trajectory generator is able to generate trajectories of smaller deviation from human trajectories.

B. Deviation Statistics

Fig. 10 shows histogram of distance from generated trajectories produced by the proposed method to the human trajectories. For comparison, the distance histogram produced by the original trajectory generator (i.e., Fig. 2) is shown in an overlapped manner. The two subfigures corresponds to the two distance measures d_1 and d_2 (refer to (4)). It can be seen from the figure that the histogram corresponding to the proposed method is more concentrated on the region of smaller distance, which means that trajectories that cannot be fitted by the original generator can be better fitted by the proposed trajectory generator.

C. Human-Like Trajectory Generation for Online Planning

1) Evaluation criteria: In order to validate that the proposed generator is able to serve a human-like trajectory planner better, we need to show that generated candidate trajectories by the proposed generator contains trajectories that are closer to the human trajectory than those generated by the original generator. However, the comparison must be conducted with the same number of candidate trajectories for the two generator, which implies equal amount of computation. We propose a scheme to evaluate the ability of a certain trajectory generator (M) to generate a human like trajectory for online trajectory planning given the number of generated candidate trajectories (K). First, denoting a trajectory set contains K trajectories as $\mathcal{T} = \{S_1, S_2, \ldots, S_K\}$, the approximating error of the trajectory set to a trajectory S is defined as:

$$E_d(\mathcal{T}, S) = \min_{i=1:K} d(S_k, S) \tag{7}$$

where d is a distance measurement between two trajectories. Then, for each human trajectory sample S, generate a trajectory set that contains K trajectories based on the trajectory generation method by enumerating K sets of free parameters. The initial states of generated trajectories should depend on the initial state of the human trajectory as we do for online planning and the generated trajectory set is denoted as $\mathcal{T}_M(K, S)$. Finally, for all human trajectories $S_1, \ldots, S_N$, we define the average approximating error as the criterion for evaluating the ability of M to approximate human trajectories under the condition of K generated trajectories:

$$C_d(M, K) = \frac{1}{N} \sum_{i=1}^{N} E_d(\mathcal{T}_M(K, S_i), S_i) \tag{8}$$

With the defined criterion, we compare $C_d(M_o, K)$ and $C_d(M_p, K)$ under $K = 3^n$, where M_o represents the original trajectory generation method and M_p represents the proposed method. Here, we need to specify how to generate K trajectories by the two methods. For M_o, we need to enumerate final longitudinal velocity v_T on uniform grids in the interval $[v_0 - d_v, v_0 + d_v]$, where v_0 is the initial longitudinal velocity of the human trajectory, d_v is set according to the extremum of $v_T - v_0$ of human trajectories (refer to II-A). For M_p, additional to v_T, α should also be enumerated (refer to III-B). It will be assigned values on uniform grids in the interval $[-d_\alpha, d_\alpha]$, where d_α is set according to the extremum of deviation scales of longitudinal velocity of human trajectories. However, since we don't know how to assign the number of grids for v_T (K_v) and α (K_α), we will generate trajectories on various settings of 2-dimensional grids, i.e., $(K_v, K_\alpha) = (3^k, 3^{n-k}), k = 0, 1, \ldots, n$, and select the setting that leads to the minimal average approximating error as the value of $C_d(M_p, K)$.

2) Resutls: Fig. 11 shows the $C_{d_i}(M_o, K)$ and $C_{d_i}(M_p, K)$ for $K = 3^n, n = 2, \ldots, 8$, where results for d_1 are in Fig. 11(a) and d_2 in Fig. 11(b) (refer to (4) for definitions of d_1 and d_2). From the figure, we see that when $n < 5$, the C value of the two methods are equal, which means that in the proposed method α is kept 0 and the grids resolution is fully devoted to the dimension of v_T. This is because when the number of grids is not big enough, enumeration of α will decrease the resolution of v_T so that the approximating precision of final velocity will degrade. Meanwhile, the phenomenon indicates that compared with α, the precision of v_T is more fundamental for generating human like trajectories. However, when $n \geq 5$, the proposed method produces smaller C values. This is because when the number of grids is big enough, the

resolution of v_T reaches saturation, so that the deviation of longitudinal velocity becomes the main factor that influences approximating precision. Using the proposed method, by enumerating α, the deviation of generated trajectories are compensated on various scales, so that the trajectory set contains trajectories that are closer to the human trajectories with various levels of deviation. According to the results, the conclusion can also be drawn that when performing online trajectory planning, if the number of generated candidate trajectories is below a threshold, we only need to enumerate v_T. Otherwise, it is better to simultaneously enumerate v_T and α on a proper setting of grids to involve trajectories that are more human-like.

V. Conclusion And Future Works

In this work, the systematic deviation of a traditional trajectory generator from human trajectories is analyzed, and the longitudinal velocity deviation is found to be the main factor. Based on the findings, a new trajectory generator is proposed, which introduces a new parameter for compensating the deviation based on a deviation profile learned from data. Experimental results show that the additional degree of freedom considerably improves the generator's fitting ability. For application in online trajectory planning, when the number of generated trajectory is high enough and with the same number of generated trajectories, the proposed generator is able to approximate the human trajectories with smaller error, which demonstrates the effectiveness of the proposed method. Besides, there might be connections between the parameter α, driving environment, and driving style, which will be studied in future works.

References

[1] J. Ziegler, P. Bender, M. Schreiber, H. Lategahn, T. Strauss, C. Stiller, T. Dang, U. Franke, N. Appenrodt, and C. G. Keller, "Making bertha drive—an autonomous journey on a historic route," *IEEE Intelligent Transportation Systems Magazine*, vol. 6, no. 2, pp. 8–20, 2014.

[2] J. Wei, J. M. Snider, J. Kim, and J. M. Dolan, "Towards a viable autonomous driving research platform," in *Intelligent Vehicles Symposium*, 2013, pp. 763–770.

[3] K. Jo, J. Kim, D. Kim, and C. Jang, "Development of autonomous car—part i: Distributed system architecture and development process," *IEEE Transactions on Industrial Electronics*, vol. 61, no. 12, pp. 7131–7140, 2014.

[4] K. Bengler, K. Dietmayer, B. Farber, and M. Maurer, "Three decades of driver assistance systems: Review and future perspectives," *IEEE Intelligent Transportation Systems Magazine*, vol. 6, no. 4, pp. 6–22, 2014.

[5] J. Wei, J. M. Dolan, J. M. Snider, and B. Litkouhi, "A point-based mdp for robust single-lane autonomous driving behavior under uncertainties," in *IEEE International Conference on Robotics and Automation*, 2012, pp. 2586–2592.

[6] J. Lu, D. Filev, and F. Tseng, "Real-time determination of driver's driving behavior during car following," *SAE International Journal of Passenger Cars - Electronic and Electrical Systems*, vol. 8, no. 2, 2015.

[7] A. Broggi, P. Cerri, M. Felisa, M. C. Laghi, L. Mazzei, and P. P. Porta, "The vislab intercontinental autonomous challenge: an extensive test for a platoon of intelligent vehicles," *International Journal of Vehicle Autonomous Systems*, vol. volume 10, no. 3, pp. 147–164(18), 2012.

[8] M. Gouy, K. Wiedemann, A. Stevens, G. Brunett, and N. Reed, "Driving next to automated vehicle platoons: How do short time headways influence non-platoon drivers' longitudinal control?" *Transportation Research Part F Psychology and Behaviour*, vol. 27, pp. 264–273, 2014.

[9] N. Abuali and H. Abou-Zeid, "Driver behavior modeling: Developments and future directions," *International Journal of Vehicular Technology,2016,(2016-12-28)*, vol. 2016, no. 2, pp. 1–12, 2016.

[10] S. Moridpour, M. Sarvi, and G. Rose, "Lane changing models: a critical review," *Transportation Letters*, vol. 2, no. 3, pp. 157–173, 2013.

[11] D. Ferguson, T. M. Howard, and M. Likhachev, *Motion Planning in Urban Environments*. John Wiley and Sons Ltd., 2008.

[12] J. Wei, J. M. Snider, T. Gu, and J. M. Dolan, "A behavioral planning framework for autonomous driving," in *Intelligent Vehicles Symposium Proceedings*, 2014, pp. 458–464.

[13] T. M. Howard, "Model-predictive motion planning: Several key developments for autonomous mobile robots," *IEEE Robotics and Automation Magazine*, vol. 21, no. 21, pp. 64–73, 2014.

[14] A. Takahashi, T. Hongo, Y. Ninomiya, and G. Sugimoto, "Local path planning and motion control for agv in positioning," in *IEEE/RSJ International Workshop on Intelligent Robots and Systems '89. the Autonomous Mobile Robots and ITS Applications. IROS '89. Proceedings*, 1989, pp. 392–397.

[15] M. Werling, J. Ziegler, S. Kammel, and S. Thrun, "Optimal trajectory generation for dynamic street scenarios in a frenét frame," in *IEEE International Conference on Robotics and Automation*, 2010, pp. 987–993.

[16] M. Werling, S. Kammel, J. Ziegler, and L. Groll, "Optimal trajectories for time-critical street scenarios using discretized terminal manifolds," *International Journal of Robotics Research*, vol. 31, no. 3, pp. 346–359, 2012.

[17] M. P. Do Carmo, *Differential geometry of curves and surfaces.* Prentice-Hall,, 1976.

[18] J. Ziegler and C. Stiller, "Spatiotemporal state lattices for fast trajectory planning in dynamic on-road driving scenarios," in *IEEE/RSJ International Conference on Intelligent Robots and Systems*, 2009, pp. 1879–1884.

[19] L. Ma, J. Xue, K. Kawabata, J. Zhu, C. Ma, and N. Zheng, "Efficient sampling-based motion planning for on-road autonomous driving," *IEEE Transactions on Intelligent Transportation Systems*, vol. 16, no. 4, pp. 1961–1976, 2015.

[20] K. Kawabata, L. Ma, J. Xue, and N. Zheng, "A path generation method for automated vehicles based on bezier curve," in *Ieee/asme International Conference on Advanced Intelligent Mechatronics*, 2013, pp. 991–996.

[21] W. Xu, J. Wei, J. M. Dolan, H. Zhao, and H. Zha, "A real-time motion planner with trajectory optimization for autonomous vehicles," in *IEEE International Conference on Robotics and Automation*, 2012, pp. 2061–2067.

[22] J. Ziegler, P. Bender, T. Dang, and C. Stiller, "Trajectory planning for bertha — a local, continuous method," in *Intelligent Vehicles Symposium Proceedings*, 2014, pp. 450–457.

[23] T. Gu and J. M. Dolan, "Toward human-like motion planning in urban environments," in *Intelligent Vehicles Symposium Proceedings*, 2014, pp. 350–355.

[24] Q. H. Do, H. Tehrani, S. Mita, M. Egawa, K. Muto, and K. Yoneda, "Human drivers based active-passive model for automated lane change," *IEEE Intelligent Transportation Systems Magazine*, vol. 9, no. 1, pp. 42–56, 2017.

[25] W. Yao, H. Zhao, F. Davoine, and H. Zha, "Learning lane change trajectories from on-road driving data," in *Intelligent Vehicles Symposium*, 2012, pp. 885–890.

[26] W. Yao, Q. Zeng, Y. Lin, D. Xu, H. Zhao, F. Guillemard, S. Geronimi, and F. Aioun, "On-road vehicle trajectory collection and scene-based lane change analysis: Part ii," *IEEE Transactions on Intelligent Transportation Systems*, vol. 18, no. 1, pp. 206–220, 2017.

[27] W. Xu, Z. Y. Wen, H. Zhao, and H. Zha, "A vehicle model for micro-traffic simulation in dynamic urban scenarios," in *IEEE International Conference on Robotics and Automation*, 2011, pp. 2267–2274.